Engineering Science and Technology, an International Journal 23 (2020) 1100–1108

HOSTED BY

Contents lists available at ScienceDirect

Engineering Science and Technology, an International Journal

journal homepage: www.elsevier.com/locate/jestch

Full Length Article

Capillary forces as a limiting factor for sawing of ultrathin silicon wafers by diamond multi-wire saw

Birgit Ryningen [a,*], Pål Tetlie [a], Sverre Gullikstad Johnsen [a,b], Halvor Dalaker [a]

[a] SINTEF Industry, 7034 Trondheim, Norway
[b] NTNU, dept. Materials Science and Engineering, 7034 Trondheim, Norway

ARTICLE INFO

Article history:
Received 26 September 2019
Revised 12 February 2020
Accepted 25 February 2020
Available online 14 March 2020

ABSTRACT

Succeeding with ultrathin silicon wafer sawing by diamond multi-wire saw, is not only a matter of optimization; the challenges of thin wafer production and the capability limit have not yet been fully understood. In this work, we have seen that regular pairing of wires occurs when the wire-wire separation distance is reduced below some critical value. The wire pairing leads to wire jumps on the wire guide rolls, and if the run is not stopped, it leads to wire breakage. Moreover, it effectively obstructs the production of wafers thinner than the critical wire-wire distance.

We suggest that the physical explanation to the observed limitations to ultrathin wafer sawing, by diamond multi-wire saw, is related to the capillary force acting on the wires due to the sawing liquid bridge connecting the wires. The hypothesis is supported by simplified mathematical modelling including capillary and spring forces between infinitely long, parallel wires. The calculations suggest that capillary forces are the main reason for wire pairing, and that wire pairing will occur when the wire distance is below some critical distance. This matches the observed, experimental behavior. The critical distance will vary with wafer saw design and operation.

To succeed with cutting very thin wafers, we recommend using lower surface tension sawing fluid or even dry in-cut, to reduce the capillary forces and thus decrease the critical wire separation distance, and to reduce wire oscillations to decrease the probability of sub-critical wire-wire separation distance. To reduce the vibration amplitude, shorter distance between the wire guide rolls, thinner wires, and increased wire tension are suggested.

1. Introduction

The photovoltaic (PV) industry is ever pushing towards less material consumption, as this will improve materials utilization and ultimately energy cost reduction. One way to reduce silicon consumption is to reduce the wafer thickness. Challenges of thin wafer production and the capability limit have, so far, not been understood [1].

Wire sawing technology has been in use by the semiconductor industry since the 1990 s. The level of research activity has increased significantly in the past decade, largely due to the global boom of the photovoltaic industry. Several research groups have looked at different aspects of wire sawing at system and process level during the last 30 years. The largest portion of research work conducted have been focused on the multi-wire slurry system, where loose silicon carbide (SiC) particles in a slurry are responsible for the material removal. The recent years' development of diamond wire sawing, where fixed diamonds on the wire cause the material removal, has shifted the research focus over to diamond wire studies. These studies have been focused on design and analysis of diamond wires since other factors in the process are assumed to be similar to those in the multi-wire slurry sawing system. Multi-wire sawing is a complex manufacturing process involving numerous different factors and their interactions. Process parameters include wire tension, wire travel speed, feed speed, SiC or diamond particle size, shapes and distribution, distribution and density of slurry or sawing liquid, pilgrim length (the length in which the wire move in one direction before it stops, and moves in the opposite direction), wire thickness and wire web density etc. Other parameters such as heat generated during sawing and vibrations will also affect sawing performance.

Several groups have studied the material removal and interaction between SiC particles, slurry and the silicon block in a rolling-indentation system [2–4]. Lately the scratching mechanisms

* Corresponding author.
E-mail addresses: Birgit.Ryningen@sintef.no (B. Ryningen), Pal.Tetlie@sintef.no (P. Tetlie), Sverre.Gullikstad.Johnsen@sintef.no (S.G. Johnsen), Halvor.Dalaker@sintef.no (H. Dalaker).

Peer review under responsibility of Karabuk University.

https://doi.org/10.1016/j.jestch.2020.02.008
2215-0986/

operation during diamond sawing has also gained attention [5–8]. The slurry wire-sawing is a three-body abrasion process, where the wafers are cut with wire going in one direction only. Diamond-wire sawing is a two-body abrasion process, where the wire is going back and forth [9]. Watanabe et al. [10] used a resin bonded diamond sawing system to investigate multicrystalline silicon cutting. They demonstrated that diamond wire sawing throughput is around 2.5 times higher than for slurry sawing, and that the saw-damage layer thickness could be reduced by a factor of two.

The reports on quality, such as mechanical strength and surface properties varies somewhat. E.g., for Czochralski (CZ) silicon wafers, Yu et al. [11] reported that "The wafers sliced by the diamond-wire saw have a greater mechanical strength than those by the conventional cutting process, beneficial for the preparation of thin wafers", whereas Wu et al. [12] concluded that the mechanical strength of silicon wafers produced by diamond wire saw is comparable to those from slurry sawing. Yu et al. [11] stated that diamond wire sawn CZ silicon wafers had smaller roughness than slurry sawn wafers, but more phase transformation of silicon was observed on diamond wire sawn wafers.

On an industrial scale, research has been focused on production rate, throughput and breakage rate. Parameter studies conducted during the last 10 years include e.g.: Würzner et al. [13] who found that higher wire velocity leads to reduced maximum crack depth, but more inhomogeneous surface roughness; and Kaminski et al. [14] who searched for the "best sawing conditions in view of reduced kerf loss, minimization of the applied forces and reduction of saw damage on the wafers". They reported that: "Thinner wires and smaller particle size distribution reduce the kerf loss and reduce the surface roughness."

The production of thinner wafers has been a hot topic due to the high potential of reduced material consumption. Ultrathin wafers down to 60 μm thickness was produced by Yu et al. (2012)[11] but no details of their set-up were published. They pointed out that "With the reduction of wafer thickness, the output parameters of corresponding solar cells become deteriorated due to the loss of the long wavelength light at some level and the recombination at the rear surface." Recent years' development of bifacial solar cells [15] might change the optimal wafer thickness with respect to solar cell performance. Experimental results with a wafer thickness of 140 μm compared to 240 μm show an improvement in efficiency [16]. Simulations indicate minimal decrease in conversion efficiency (0.6 percentage points) from decreasing the wafer thickness from 200 μm to 58 μm [17]. The optimal thickness is therefore a trade-off between material consumption, solar cell performance, and handling. It will also depend on solar cell concept and module concept. Further studies are, however, needed to conclude [15].

H. Wu (2016)1 concluded in a recent review article about wire sawing technology, that even though extensive research work has been carried out in wire sawing technology (both modelling and experimental studies), effective guidelines for wire sawing performance and optimization are still lacking. Fundamental investigations of the wire saw systems, process parameters, materials, and their interactions are still needed to achieve full understanding.

Unforeseen challenges in the production of thin wafers were experienced at SINTEF as we were asked to deliver sub-100 μm wafers to a research project as reference material for exfoliated Si. Although high success rate was achieved in producing 140 μm wafers, several unsuccessful attempts were made to produce 100 μm wafers. None of the adjustments implemented in the sawing process could prevent wire-pairing and subsequent wire breakage and wafer cracking. Hence, wafering of 100 μm wafers seemed to be unfeasible regardless of machine settings, which was unexpected since this wafer thickness is not far below industrial state of art.

This led to the hypothesis that there is a fundamental lower limit to wafer thickness. This paper explores a plausible explanation, based on capillary attraction between neighboring wires, for the observed, apparent limit to wafer thickness. The paper proceeds with a brief introduction to the experimental methods, materials, and observations, theoretical considerations and discussion. The aim of the paper is to contribute to a more fundamental understanding of one of the limiting aspects of wire sawing, namely the minimum wafer thickness achievable by wire sawing.

2. Experimental methods and materials

In multi-wire sawing, the silicon block is mounted on a plate of glass or other material, on a downward moving table. It is then pushed onto a web of wires, where the sawing is performed by grits either fastened to the wire (as in diamond wire sawing) or suspended in the sawing fluid (as in SiC slurry sawing). A simple schematic drawing of the wire guide rolls and the block as well as some pictures of the current set-up are shown in Fig. 1.

In this work, an industrial scale multi-wire saw (Meyer Burger DS265/4), was used to cut high quality monocrystalline silicon blocks of various dimensions. This saw was originally designed for slurry-based wafering but was equipped with diamond implanted wire from Asahi Diamond Industrial Co. with dimensions given in Table 1.

A modified sawing liquid distribution system (seen in Fig. 1B) was designed to distribute the sawing liquid more evenly and apply it to the wire web closer to the ingot. This set-up seemed to be more robust than the original distribution system and was used in all cuts after it was installed. Water-based and tripropylene methyl glycol ether (DowanolTM, Dow Chemical Company) based slurries were utilized. The surface tension of the tripropylene methyl glycol ether and water are listed in Table 2.

To ensure optimal sawing conditions, the saw was thoroughly cleaned prior to every run, and the web was checked for wire twists. Additionally, the web was run for an hour prior to sawing, to heat the web. A brief summary of details regarding the experimental runs is given in the Appendix (see Table A).

The wire saw was set-up for production of wafers of 140 and 100 μm thickness by choosing different wire and wire guide-rolls. The pilgrim and the distance between the wire guide rolls were the same for all the runs, and for a given target wafer thickness, the same wire pitch and wire dimensions were used. These numbers are summarized in Table 1. A base-line set-up was defined, and the details are summarized in Table 3 and Fig. 2.

Due to the persistent failure to produce 100 μm wafers, several hypotheses to explain the failure were put forward and tested, resulting in some modifications to the sawing process. Modification to the baseline settings included:

- Reductions in table speed, wire speed, and sawing liquid flow-rate. Since the baselines for these parameters were chosen close to the machine maximums (in order to approach an industrial situation where high throughput is a key factor), no tests were done with increases beyond the base settings.
- Re-grooving of the wire guide rolls at two different suppliers, using milling and a lathe, to eliminate the possibility that the wire pairings could be due to worn or sub-optimal grooves on the wire guides.
- Split in the web: a gap of 4–5 mm in the wire web was intentionally introduced at the edge of the block, such that the last wafer was of ≈1 mm thickness. This was to avoid the risk that small fragments of the block or wafer pieces would be shaved off at the end of the block. Likewise, the first wafer was also made ≈1 mm thick by intentionally positioning the other edge slightly outside the web.

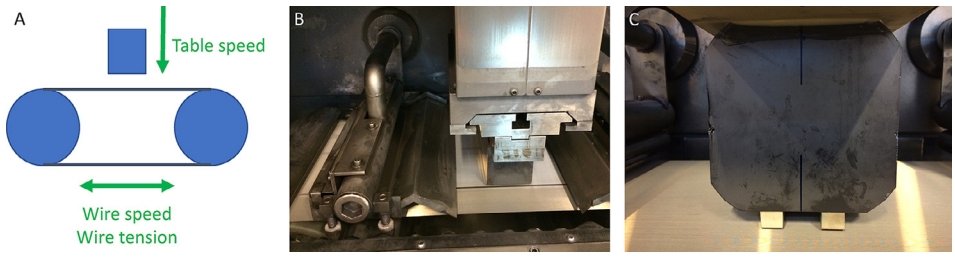

Fig. 1. A: Schematic drawing of the block and wire guide rolls with some of the sawing parameters shown in green. B: A photo of the modified sawing liquid system. C: A photo of a silicon block with strips attached to the bottom for a smoother start.

Table 1
Parameters kept constant across all runs with 100 μm and 140 μm thick wafers.

Wafer thickness, μm	Wire diameter, μm	Diamond size, μm	wire-wire separation distance μm	Pilgrim, m	Distance between wire guide rolls, mm
100	120	10–20	250	500–466	700
140	100	10–20	262	500–466	700

Table 2
Surface tension of water and sawing liquid.

Sawing liquid	Surface tension liquid–air
Tripropylene methyl glycol ether [18]	0,03 J/m^2
Water	0,072 J/m^2

Table 3
Base-line sawing parameters. Initial phase corresponds to the first 3 mm of the cut; Main phase refers to the remaining part of the cut.

Parameter	Value		Unit
	Initial phase	Main phase	
Table speed	0.4	0.7	mm/min
Wire speed	7	14	m/s
Sawing liquid flowrate	5000	6500	kg/h
Wire tension	24	24	N

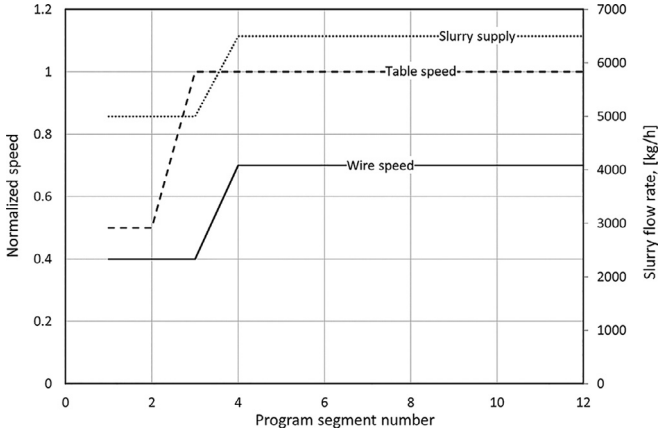

Fig. 2. An example of how the wire speed, table speed and sawing liquid supply may be changed through a run. For the baseline run, the maximum table speed was 1 mm/min and maximum wire speed was 14 m/s. Program segment number indicating the different stages in the run.

- Tilted block to get a smoother transition from "not cutting mode" to "cutting mode". The block was slightly tilted around an axis perpendicular to the movement directions of the wire, Fig. 3.
- Initially, strips were attached at the bottom of the block (Fig. 1C) to smoothen the in-cut phase. This strategy was, however, quickly discarded. Some of these strips were carried, by the wires, to the wire guide rolls and caused wire jumps.

A total of 6 runs to produce 140 μm wafers and 8 runs to produce 100 μm wafers were conducted. 140 μm thick wafers were in general made without any problems, regardless of which set-up we used, however none of the attempts to produce 100 μm wafers were successful. The difference in results were of such an essential character that we decided to investigate the fundamental limits for sawing thin wafers by a theoretical approach, since our experiments clearly indicate a fundamental barrier between producing 100 and 140 μm wafers.

3. Experimental observations

8 attempts at 100 μm were conducted and all of them had wire breakage just 2–3 mm after in-cut. Inspection of the failed runs at 100 μm revealed some common features (see Figs. 4 and 5):

- Extensive and regular wire pairing was observed in all the attempts.
- The double-grooves appear from the very start of the cut, indicating that wires pair up prior to entering the block, or just as they are entering the block.
- None of the set-ups (baseline and modified set-ups) were able to avoid wire pairing.

The pairing of wires tends to obey a repeatable pattern, as illustrated in the highlighted region "1″ in Fig. 4. That is, pairing starts at the edge of the wire web and propagates throughout the wire mesh. A few wires remain unpaired, however, and occasionally, three wires may join, as seen in the highlighted regions "2″ and "3″ in Fig. 4. From the cutting grooves, it seems that two joined wires can sustain stable sawing at slightly increased speed compared to a single wire. When three wires join however, this leads to even greater increase in sawing speed, zig-zag patterns, instabilities of the web (e.g. wire jumps on the wire guide rolls), wafer breakages, and eventually wire breakage.

4. Theoretical considerations and calculations

Walters et al. [19] reported similar regularity in wire pairing and a thick/thin signature in thin wafers, but no explanation to the phenomena was given.

From the calculation presented below, we propose that this limit is related to a critical wire-wire distance beneath which wire pairing is likely to occur.

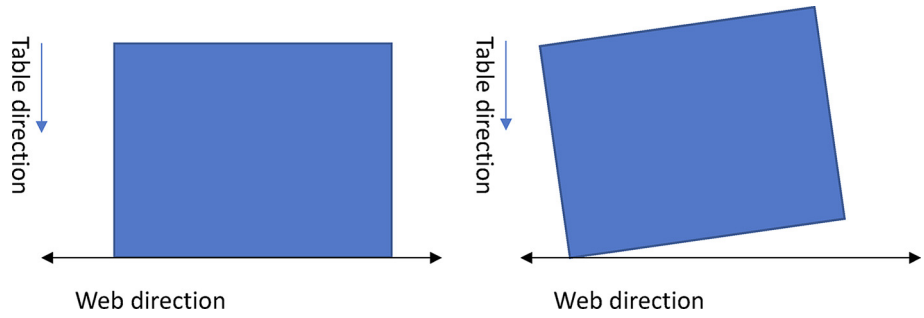

Fig. 3. Schematic of tilted block and the effect of the initial cutting length.

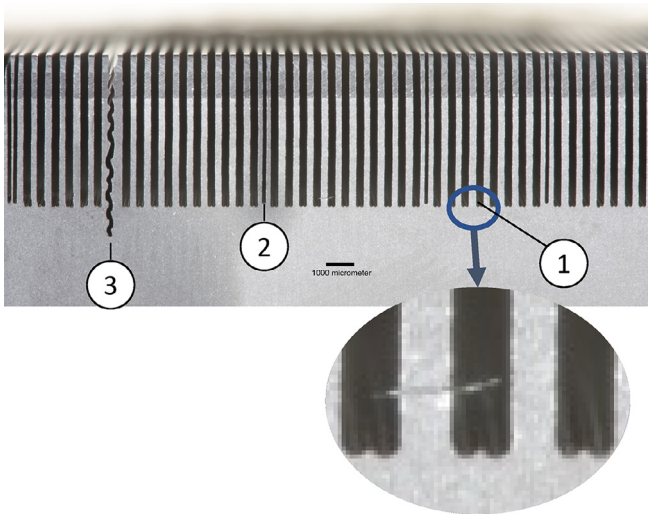

Fig. 4. Picture showing a block where the wires have paired up mainly two-and-two. As seen in the enlarged circle, most of the grooves are made by two wires (1). A few single-wire grooves (2) and one zigzagged multi-wire groove (3) are also shown.

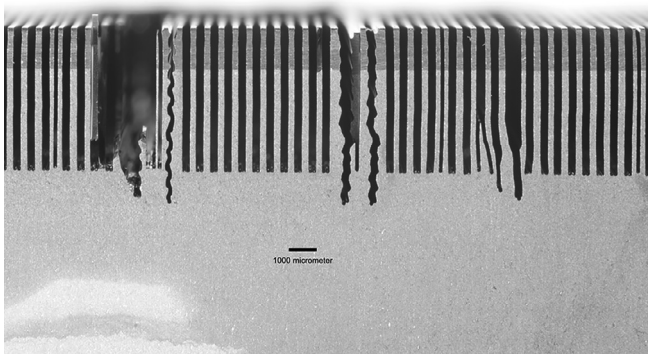

Fig. 5. Examples of the sawing result when more than two wires pair up. The sawing speed is significantly increased, and the track becomes zigzagged. This results in instability of the web, wire jumps on the wire guide rolls, wafer breakages, and wire breakage. There was a wire break after approximately 5 mm in this run.

Furthermore, we suggest that the reason for wire pairing is wire-wire attraction due to capillary force caused by sawing fluid bridging the gap between the wires. The critical distance is thus related to wire and sawing fluid material properties and atmosphere as well as wire tensile stress and vibrations. In this case, mere adjustment of the existing sawing system will most likely not be enough to overcome the wafer thickness limit – rather, fundamental modifications to the sawing process (e.g. to reduce vibrational amplitude) or careful selection of wire and sawing liquid materials, and atmosphere (e.g. to reduce attractive capillary forces) will be required.

The wire deformation due to wire sawing force is not considered in this article. To obtain deeper understanding of the process leading to deformation and fracturing in silicon wafers and steel wires, a thorough analysis of the cutting zone on several scales is needed (see e.g. Maruschak et.al. [20]). This is, however, outside the scope of the current investigation.

During cutting, the individual wires of the multi-wire saw will experience significant stress and strain from a variety of sources. In order to investigate the hypothesis that capillary forces are responsible for wire pairing and a limiting factor in minimum wafer thickness, a discussion on the forces in the system is needed.

The following is a description of the spring and capillary forces acting between two long, parallel, horizontal wires, which will allow us to explore the force balance for different wafering set-ups. This simplified model will be used to explain the wire pairing.

4.1. Spring Force

We consider a cylindrical wire of length, L_0, and radius, r. The wire is being deformed by a force acting perpendicular to its length axis, at its mid-point (see). The point of attack (PoA) is pulled away from the equilibrium position and the sum of the spring forces, $F_{\|}$, balance the deforming force, F, exactly. The deformation is characterized by the PoA being translated a distance δ away from its equilibrium position. If the endpoints of the wire are fixed in space, the deformation results in the wire being stretched to the new length L, which is given by Pythagoras' theorem and is related to the angle of deformation, β;

$$L = L_0\sqrt{1+(2\delta/L_0)^2} = \tfrac{2\delta}{\sin\beta}\,. \tag{1}$$

The magnitude of the deforming force can now be expressed as

$$F = 2F_{\|}sin\beta = 2k\left(1-\frac{L_0}{L}\right)\delta, \tag{2}$$

where $k \equiv AE/L_0$ is the spring constant, A is the wire cross-sectional area, and E is the elastic modulus. Considering that the deformation is small compared to the length of the wire, $(2\delta/L_0)^2 \ll 1$, we may, from Eq. , write $L_0/L \approx 1-2(\delta/L_0)^2$, where higher order terms of the Taylor expansion of the square root were neglected. Thus, we may express the deformation force as a function of the deformation, δ, and wire properties;

$$F \approx \tfrac{4\pi r^5 E}{L_0^3}\left(\tfrac{\delta}{r}\right)^3\,. \tag{3}$$

4.2. Capillary force

Princen (1969) investigated capillary forces between assemblies of vertical and horizontal [21–23] cylinders in the absence of gravity. Cooray gave a discussion of capillary bridges between horizontal, parallel cylinders under the influence of gravity [24]. We only consider wire-wire distances and wire radii much smaller than the capillary length, $l_0 \equiv \sqrt{\Delta\gamma/(\Delta\rho g)}$ ($\approx 2.7mm$ for water–air-steel), where $\Delta\gamma \equiv \gamma_{sl} - \gamma_{sv}$ is the liquid–vapor interfacial tension, γ_{sl} and γ_{sv} are the solid–liquid and solid–vapor interfacial tensions, $\Delta\rho$ is the density difference between the liquid and vapor, and g is the gravitational acceleration. We thus neglect gravity and assume that the capillary bridge connecting the wires is symmetrical about the center-center plane. The capillary pressure inside a liquid column connecting two parallel cylinders surrounded by vapor (See Fig. 6), is thus given by

$$P_c = P_0 - \gamma/R\ , \tag{4}$$

where P_0 is the pressure outside the liquid column,

$$\gamma = \frac{\Delta\gamma}{\cos\theta}\ , \tag{5}$$

is the surface tension, θ is the wetting angle,

$$R = r\left(\frac{1+d/r-\cos\alpha}{\cos(\theta+\alpha)}\right)\ , \tag{6}$$

is the curvature radius of the liquid–vapor interface (meniscus), and d is half the cylinder-cylinder separation distance. For angles $\theta+\alpha > \pi/2$, the resulting curvature radius will be negative. This implies that the surface is convex outwards and results in a positive gauge pressure between the cylinders, hence a repulsive force pushing them apart. For angles $\theta+\alpha < \pi/2$, on the other hand, the resulting curvature will be concave (as indicated in Fig. 6) and cause a negative gauge pressure, hence an attractive force between the cylinders.

The excess force per unit length, exerted on the cylinder surface by the liquid column, due to capillary pressure, is given by

$$F_c = L_c r\int_0^{2\pi}(P_0 - P_c)\cos\phi d\phi = 2L_c r\int_0^{\alpha}(\gamma/R)\cos\phi d\phi, \tag{7}$$

where end effects have been neglected, implying that the length of the liquid column is much larger than the distance between the cylinders, $L_c \gg d$. A positive force indicates attraction between the cylinders and negative force indicates repulsion. Solving the integral and inserting Eq. for R gives the scaled capillary force acting in the horizontal direction as:

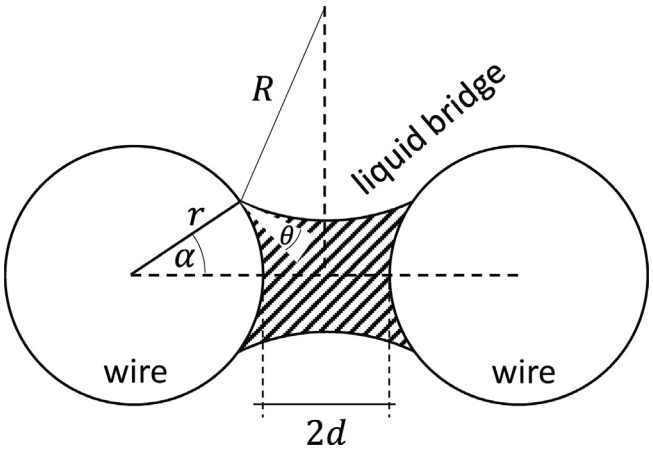

Fig. 7. Schematic of the cross-section of two parallel, cylindrical wires of radius r, connected by a liquid bridge. The liquid bridge is assumed to be symmetrical about the center-center plane and intersects the wire surface at the angle α due to the wetting angle θ. This results in a curvature radius of R for the liquid meniscus.

$$F_c/L_c r\gamma = \frac{2\sin\alpha\cos(\alpha+\theta)}{1+d/r-\cos\alpha}\ . \tag{8}$$

Princen (1970) [23] showed that there is a relationship between the curvature radius, R, cylinder radius, r, and intersection angle, α,

$$\left(\frac{R}{r}\right)^2\left[\frac{\pi}{2}-\theta-\alpha+\sin(\theta+\alpha)\cdot\cos(\theta+\alpha)\right] + 2\left(\frac{R}{r}\right)[\sin\alpha\cdot\cos(\theta+\alpha)-\alpha\cdot\cos\theta]+\sin\alpha\cdot\cos\alpha-\alpha=0, \tag{9}$$

where it was assumed that the shape of the liquid bridge cross-section only depended on d/r and θ. This implies that adding liquid to the column increases L_c, but does not affect the shape of the liquid column cross-section.

The dimensionless cylinder separation, d/r, as a function of the liquid-cylinder intersection angle, α, is obtained from Eq. (6)

$$\frac{d}{r} = \left(\frac{R}{r}\right)\cos(\theta+\alpha)+\cos\alpha-1. \tag{10}$$

It is noted that for two-cylinder systems, no physically meaningful solutions to Eq. are found for vapor-wetted cylinders ($\theta \geq 90^{\circ}$). The condition for mechanical stability is that[23]

$$\alpha < \alpha_0\ , \tag{11}$$

where

$$\alpha_0 = \arcsin\left(\frac{\sin\theta}{1+d/r}\right)-\theta\ . \tag{12}$$

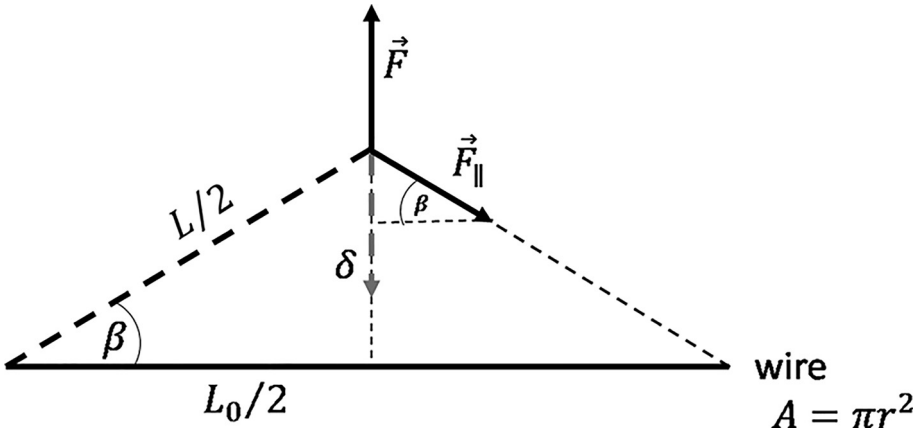

Fig. 6. Schematic of geometry and force balance on a wire that is being pulled away from equilibrium by a force, $\vec{F}$, acting perpendicular to its length axis. At steady state, the sum of the spring forces pulling in opposite directions from the point of attack, $\vec{F}_{\parallel}$, balances the deforming force exactly.

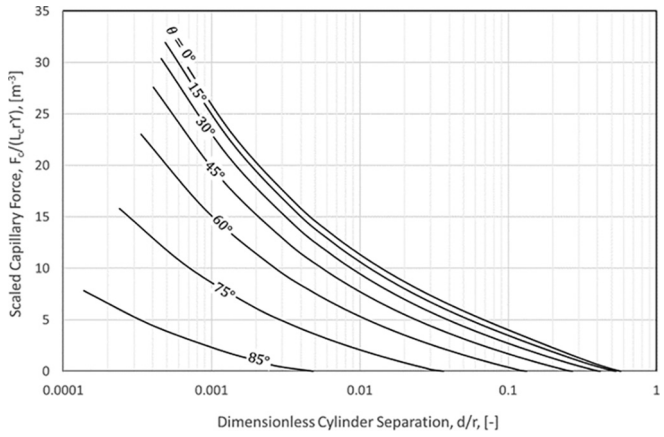

Fig. 8. Scaled capillary force, $F_c/(L_c r\gamma)$, as a function of dimensionless separation distance between two long, parallel cylinders connected by a liquid bridge, but surrounded by vapor. Positive force indicates attraction between the cylinders, whereas negative force indicates repulsion.

Thus, the solution to Eq. corresponding to the condition Eq. , is the physically valid solution.

In Fig. 8, the excess force scaled with liquid column length, cylinder radius, and surface tension, is shown as a function of dimensionless cylinder separation distance, for selected wetting angles. It is seen that the capillary force decreases with the separation distance and for increasing wetting angle. Moreover, it is seen that for a given wetting angle, the capillary force is attractive beneath some critical separation distance.

5. Discussion

The regularity and the high degree of symmetry with which wire pairing occurs makes it clear that it is not a random phenomenon, but rather the rule when the wafer thickness is reduced to 100 μm in the current sawing set-up. Hence, we chose to investigate the possible root of cause by theoretical calculations.

Although the sawing process was not observed visually by e.g. high-speed camera, it is clear from the grooves seen in Figs. 4 and 5 that wire pairing was already established prior to the wire web actually touching the silicon block.

It might be speculated that conditions during the very start of the cut was to blame. Reductions in wire speed and table speed, as well as tilting of the block and the mounting of strips (Fig. 1) were attempted to give a smoother transition into the cut, but none of these modifications had any noticeable effect and the problems with wire-pairing persisted. The fact that the saw had previously been used for slurry-based wafering could mean that some SiC was left in the interior of the saw. The saw was thoroughly cleaned before installation of the diamond wires as well as prior to each experimental run. Despite this, it cannot be ruled out that SiC particles may be present and get lodged in the guide rolls, causing a disturbance in the wire behavior and initiate wire pairing. However, it seems unlikely that such events would occur with any consistency. Except for possible isolated incidences, it is expected that this effect is secondary.

The temperature in the cutting zone is not controlled by other means than by using the sawing fluid as coolant. The temperature in the cutting zone is, nevertheless, expected to increase during sawing. This may lead to viscosity change in the sawing fluid, overheating of the silicon and/or the wire. Even though this is believed to be important, it is not regarded as a likely explanation in this case, since the pairing of wires are believed to occur prior to the actual cutting starts.

Another possible explanation is that twisting of wires might lead to instabilities in the wire web. The wire twist was measured occasionally and was found insignificant. Hence, this explanation was discarded.

None of the phenomena outlined above seem to be able to explain the difficulties associated with cutting 100 μm wafers, compared with cutting 140 μm wafers. Nor can they explain the regular and symmetric wire pairing observed when cutting at 100 μm.

The derivations above show that the attractive capillary forces between two horizontal cylinders connected by a liquid bridge increase steeply for decreasing separation distance (Fig. 8). This indicates that the attractive capillary forces between two wires will be much greater in the 100 μm case than in the 140 μm case, if the wire radius and material as well as sawing fluid and

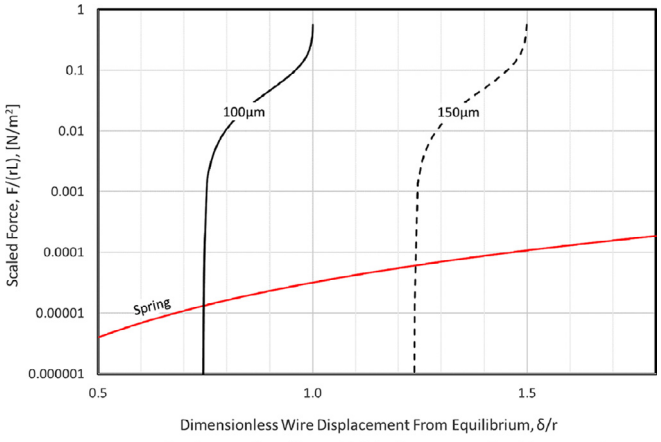

Fig. 10. Comparison of scaled capillary ($\theta = 45^{\circ}$) (black) and spring (red) forces, as functions of dimensionless wire displacement from equilibrium position. Capillary forces are shown for two equilibrium situations with initial wire-wire distances of 100 μm (solid) and 150 μm (dashed), for 100 μm diameter steel wires with a water bridge. Two-wire systems were assumed, with symmetric displacement of the two wires.

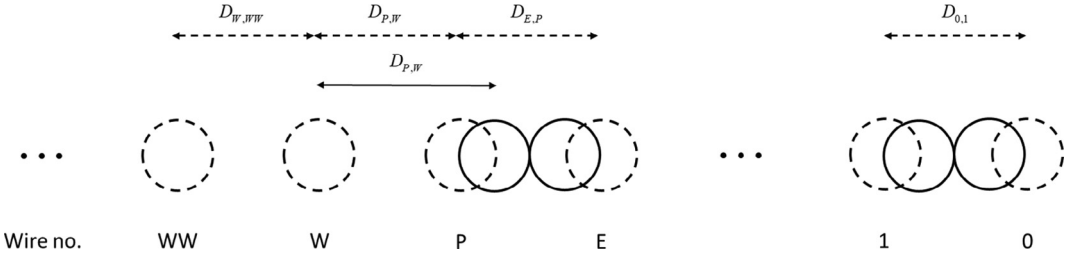

Fig. 9. Sketch of a cross-section of the wire web with wires numbered from the edge. Solid lines indicate situation after (partial) pairing; dashed lines indicate initial condition with equispaced wires.

atmosphere are the same. Thus, separation distance-dependent capillary attraction may explain the increased tendency of wire pairing observed in the 100 μm runs, compared with the 140 μm runs. E.g., a wire P paired with its neighbor E will be displaced away from its initial position, hence increasing the separation distance to its neighbor W (see Fig. 9). If the distance between W and P becomes larger than the distance between W and WW, the net force on W will cause it to be attracted to and paired with WW. Moreover, since the outer wires, at the edge of the web (Wire 0 in Fig. 9), lacks one neighbor, there is no force to balance the attractive capillary force from its single neighbor. Hence, it is probable that pairing will commence at one or both web edges. This will disturb the capillary force balance between neigh boring wires and set off a chain reaction of wire pairing that propagates through the wire web.

The attractive capillary force between liquid connected wires is thus a plausible candidate for the cause of the wire pairing. It depends on physical properties and parameters (e.g. wire spacing and sawing fluid surface tension) rather than random events, which is in line with the regularity of the phenomena observed.

In Fig. 10, the scaled attractive force due to capillary pressure (Eq.) is compared to the restoring spring force (Eq.(3)) for two different hypothetical scenarios (initial separation of 100 μm and 150 μm), for 100 μm diameter steel wires with a water bridge and wetting angle of $\theta = 45^{\circ}$. It is immediately seen that the capillary force, except for in a very small interval, is orders of magnitude larger than the spring force, in the attractive regime. That is, if the wire displacement becomes larger than the critical value, where the capillary and spring forces are equal in magnitude, the wires are bound to collapse together. Furthermore, it is seen that the critical displacement is sensitive to the initial separation distance. That is, for larger initial separation distances, the dimensionless critical displacement is increased. E.g., the critical displacement is larger for the 140 μm case than for the 100 μm case, due to its larger initial separation distance. In Fig. 11, it is seen how increasing the wetting angle of the liquid bridge will result in increased critical wire displacement, for a 100 μm diameter steel wire with initial wire-wire separation distance of 100 μm. The spring force is negligible (not shown in the figure) so the critical displacements are found where the curves intersect the horizontal axis. It is noted that below the critical wire displacement, two situations may occur: 1) the capillary pressure is negative, causing a weak attractive force between the wires, and 2) the capillary pressure is positive, causing a weak repulsive force between the wires.

Fig. 12 shows the results of the calculations using dimensions relevant for cutting 100 μm and 140 μm wafers on the DS265/4

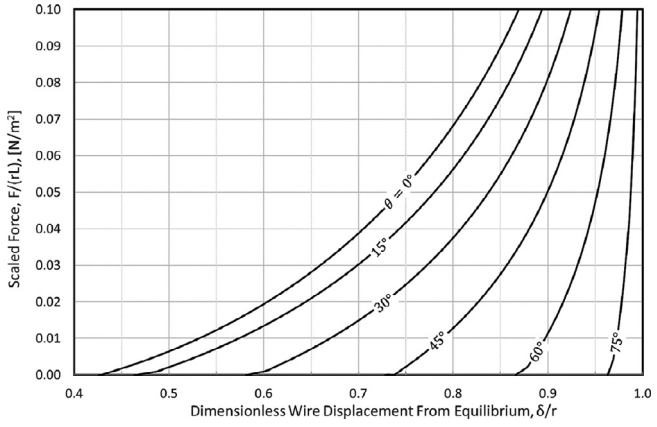

Fig. 11. Comparison of scaled capillary forces, for selected wetting angles, for water, for 100 μm initial separation distance and 100 μm diameter steel wire.

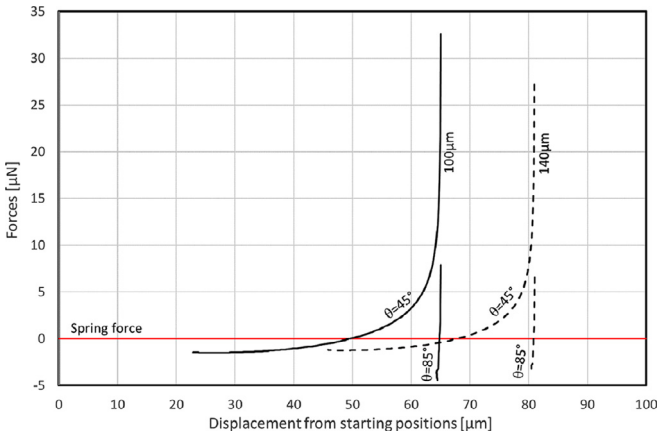

Fig. 12. Capillary forces as function of displacement from starting position for wetting angles θ = 45° and 85° for 100 μm (solid) and 140 μm (dashed) wafer thickness. The spring force is approximately zero and is shown as a red line. Positive force indicates wire attraction whereas negative force indicates wire repulsion.

wire saw, using data from Tables 1–3. Elastic modulus of $E = 2.0 \cdot 10^{11} Pa$ (steel) was used for the wires. As described previously, the capillary forces become attractive and rapidly increase once a critical displacement is reached. When cutting 140 μm wafers, the initial spacing between two wires is 162 μm, whereas when cutting 100 μm wafers it is only 130 μm. The critical displacement for collapse of the two wires depends on the wetting angle of the fluid used, but as an example, θ = 45° and θ = 85° are used in Fig. 12. θ = 85° represents the case where there is very little attraction between the wires and the critical displacement corresponds to the two wires almost touching. For the intermediate case of θ = 45°, the critical displacement is 49 μm for the cutting of 100 μm wafers and 68 μm for 140 μm wafers, respectively.

The derivations were done for a two-wire system where the displacement of the two wires was symmetric about their common mass center. The way the liquid bridge is sketched in Fig. 7, there will be no direct capillary force between wires that are not closest neighbors, since the liquid bridge is discontinuous. There would, however, be an indirect effect of including more wires, since they would make the system stiffer, in the sense that a greater force would be required to pull a wire out from its equilibrium position. However, due to the short range of the attractive capillary force, it can be expected that the many-wire effect is of second order.

A plausible explanation is therefore that at the low initial distances between the wires necessary to cut 100 μm wafers, the lateral displacement of the wires during operation are large enough to bring two neighboring wires within the critical distance of one another. At 140 μm the critical distance is significantly larger, and thus the displacements are not enough to lead to wire pairings on a regular basis.

The entire sawing process and the processing region are inevitably subject to vibrations, which could be responsible for the supercritical sideways displacement of the wires. Vibrations in the saw and wire web are reported to affect the product processing quality and the processing efficiency in many ways; bow and bending of the wafers, non-parallel sides, total thickness variation (TTV), cutting margin waste, the damaged layer thickness and wafer surface roughness [25]. The considerations presented here indicate that in addition, the amplitude of the vibration will set a limit to how thin the wafers can be cut.

Zhu and Kao [26] studied wire vibrations in a wire-slurry system. They concluded that the vibration amplitude of the wire is larger for a smaller contact span between block and wire, i.e. if the

block is tilted, as in our cases, the vibrations are larger than for a block meeting the wire web with the whole surface at once. Tilting was still chosen since the silicon block surface is mirror polished and wires could easily slide sideways when the block is pushed to the wire web. However, we concluded that the pairing of wires happens before the block enters the web, and the tilting angle will therefore be of no importance. To dampen the vibrations Zhu and Kao [26] suggest increasing the contact span between ingot and web (smaller tilt angle) or increase the wire tension. The latter is also reported by Huang et al. [27]. Compared with the tension of the wire, Zhu and Kao reports that the wire speed is of minor importance in affecting the tool vibration characteristics in the wire sawing process, whereas Huang et al. reports that the amplitude decreases with tension and increases with wire speed.

In the present work the wire tension was 24 N, which is close to the limit of the saw (25 N), and the wire speed was 14 m/s, with a slower start, typically 7 m/s. With the set-up that Huang et al. were using, they could have expected a vibrational amplitude (RMS) of well above 100 μm for our values of wire tension and wire speed. Our systems cannot be compared directly, especially since they used a saw with only one wire and different wire thickness (250 μm), but their results may still give an indication of the vibrational magnitude that can be expected, which is of the same order of magnitude as the critical displacements found in our calculations. It is noted that the DS265/4 saw has a relatively long distance between the wire guide rolls (700 mm) compared to new saws. This makes vibrations in the wire web more pronounced and more difficult to control.

According to the presented calculations, the spring force that counteract the attractive capillary force between the wires is influenced by both the distance between the wire guide rolls and the wire thickness. Compared to the capillary force, however, the spring force is so small that this will not influence the overall force balance. However, both the wire tension and the distance between the wire guide rolls will influence the vibrations in the web and are thus still important parameters for the cutting of thin wafers. The basic amplitude of a vibration is given by $= D/F$, where A is the amplitude, D is the distance travelled and F is the frequency. That is, for a given frequency, the amplitude of a wave will increase linearly with travelled distance, which in our case is given by the wire guide roll distance.

It must be noted that the calculations presented are for a static case and does not include wire momentum due to the vibrations, which may even help pull wires away from each other and perhaps even separate wires that have paired. This should be considered in a complete and more detailed investigation of the onset of the wire pairing.

Given the above indications from other studies [25–27] and the presented calculations and experimental results, it is tentatively concluded that the reason for failure is that sawing of 100 μm thick wafers is very close to what can, theoretically, be achieved with the DS265/4 saw.

Given the indications of the order of magnitude of vibration amplitude that can be expected, it is proposed that the vibrations will provide the displacement necessary for the capillary forces to cause a collapse. The smaller the wetting angle, the smaller the displacement necessary to obtain wire pairing. For a wetting angle of $\theta = 45°$, a displacement of less than 50 μm will result in wire pairing in a static system. Even if we consider the moment of inertia associated with the oscillating wires, it is plausible that wire pairing can be explained by the combination of displacement due to vibrations and capillary forces.

To lower the minimum possible wafer thickness for a given set-up, several courses of action can be taken. Either, the capillary forces can be decreased e.g. by using a lower surface tension sawing fluid and thus also decreasing the critical wire-wire separation distance, or the vibrational amplitude of the wires can be decreased to keep the wire displacements below the critical displacement. To reduce the vibration amplitude, shorter distance between the wire guide rolls, thinner wires and increased wire tension are suggested.

The calculations also show that increasing the wire tension does not significantly affect the force balance between spring- and capillary forces (although it may have an indirect effect by reducing amplitude of oscillations).

It could also be possible to perform a dry in-cut, where the start of the cut will be conducted with no sawing fluid at all, or even a web that is fully immersed in the sawing liquid or some other soft matter. This would give no capillary forces that can cause wire pairings but might introduce other challenges that need to be overcome. To avoid overheating in the case of dry in-cut, sawing fluid will probably need to be applied immediately after the wires have started scratching the silicon block.

6. Conclusion

Silicon wafers have successfully been produced at 140 μm thickness on a multi-wire saw, whereas seven attempts to cut 100 μm wafers all failed. In all attempts there was wire breakage after only 2–3 mm. Examinations of the failed attempts show regular wire-pairings occurring prior to or at the start of the in-cut.

A simplified model of capillary forces and spring forces have been presented and used to explain these observations and to study the limitations to ultrathin wafer sawing by diamond multi-wire saw. These calculations show that capillary forces between wires in a multi-wire saw are very sensitive to wire distance, and that once the separation drops below a certain critical limit, the capillary forces become strongly attractive and several orders of magnitude greater than the restoring spring forces.

It is therefore believed that wire-pairing due to capillary forces is a limiting factor in the production of thin wafers with multi-wire saw. The critical thickness is expected to be system specific. For the current set-up, it appears to lie in the range 100–140 μm.

The calculations indicate that reduced surface tension in the sawing liquid, or even dry in-cut, as well as reducing the vibrational amplitude in the wires may allow for production of thinner wafers.

Declaration of Competing Interest

The authors declare that they have no known competing financial interests or personal relationships that could have appeared to influence the work reported in this paper.

Acknowledgements

The laboratory work was funded by the EU project Cost-reduction through material optimization and Higher EnErgy outpuT of solAr pHotovoltaic modules (CHEETAH) - joining Europe's Research and Development efforts in support of its PV industry, EC Grant Agreement n°609788. The calculations were funded by the researcher project DIAmond sawing and surface treatment of high performance Multicrystalline silicon wafers for high efficiency solar cell APPlications (DiaMApp), funded by the Research Council of Norway. Special thanks to NorSun AS for discussions and for supplying material. The authors are grateful for fruitful discussions with Børge Holme, Eivind Johannes Øvrelid, and Stein Tore Johansen at SINTEF Industry.

Appendix

Table A: Short summary of all runs

Run	Wafer thickness [μm]	Wire pairing [Yes/No]	Modification	Nozzle design	Notes
1	140	Y		Original	Wire pairing after 2 cm
2	100	Y	Strips glued to block.	Original	Wire breakage due to wire pairing after few mm
3	100	Y		Original	Wire pairing after few mm
4	100	–	Tilted ingot	Original	Broken wafer pieces imbedded in guide roll from experiment 3
5	140	N		New	Good run.
6	140	Y		New	Wire pairing after 14 cm and wire breakage.
7	140	N		New	Good run
8	140	N		New	Good run
9	140	N		New	Wire breakage
10	100	Y		New	Wire breakage after 5 mm cutting.
11	100	Y	Increased cut-in sequence from 2 mm to 8 mm. Reduced coolant flow to 4000.	New	Wire pairing and breakage after 6.4 mm.
12	100	Y	Reduced wire speed. Reduced feeding rate. (0.35 mm initially, 0.6 mm main cut) Reduced coolant flow to 4000.	New	Wire pairing after 6 mm.
13	100	Y	Reduced wire speed. Reduced feeding rate. Reduced coolant flow	New	Wire jumps after 5 mm, reducedblock.
14	100	Y	Reduced wire speed. Reduced feeding rate. Reduced coolant flow	New	Wire jumps after a 5 mm,reduced block.

References

[1] H. Wu, Precis. Eng. 43 (2016) 1–9, https://doi.org/10.1016/j.precisioneng.2015.08.008.
[2] H.J. Möller, phys. stat. sol. (a) 203 (4) (2006) 659–669, https://doi.org/10.1002/pssa.200564508.
[3] A. Bidiville, K. Wasmer, J. Michler, P.M. Nasch, M. Van der Meer, C. Ballif, Prog. Photovolt: Res. Appl. 18 (2010) 563–572, https://doi.org/10.1002/pip.972.
[4] C. Yang, F. Mess, N.M. Shreyes, S. Danyluk, Adv. Mater. Sci. Appl. 2 (4) (2013) 138–143, https://doi.org/10.5963/AMSA0204002.
[5] E. Cai, B. Tang, W.R. Fahrner, L. Zhou, European Photovoltaic Solar Energy Conference and Exhibition, Hamburg, Germany, 2011. Doi: 10.4229/26thEUPVSEC2011-2BV.4.28.
[6] H.J. Möller, R. Buchwald, S. Winstanley In: 6th International Workshop on Crystalline Silicon Solar Cells (CSSC6) Aix-les-Bains, France, 2012.
[7] A. Kumar, S.N. Melkote, S. Kaminski, C. Arcona, J. Am. Ceram. Soc. 100 (2017) 1350–1359, https://doi.org/10.1111/jace.14732.
[8] Z. Zhang, D. Guo, B. Wang, K. Kang, B. Zhang, Scien. Rep. 5 (2015) 16395, https://doi.org/10.1038/srep16395.
[9] A. Bidiville, K. Wasmer, R. Kraft, C. Ballif, European Photovoltaic Solar Energy Conference and Exhibition, Hamburg, Germany, 2009. Doi: 10.4229/24thEUPVSEC2009-2CV.1.86.
[10] N. Watanabe, Y. Kondo, D. Ide, T. Matsuki, H. Takato, I. Sakata, Prog. Photovoltaics Res. Appl., 2010, 18, 485–90 doi: 10.1002/pip.923.
[11] X. Yu, P. Wang, X. Li, D. Yang, Sol. Energy Mater. Sol. Cells 98 (2012) 337–342, https://doi.org/10.1016/j.solmat.2011.11.028.
[12] H. Wu, S.N. Melkote, S. Danyluk, Adv. Eng. Mater. 14 (2012) 342–348, https://doi.org/10.1002/adem.201100263.
[13] S. Würzner, A. Falke, R. Buchwald, H.J. Möller, Energy Procedia, 2015, 77, 881–890 doi: 10.1016/j.egypro.2015.07.124.
[14] S. Kaminski, R. Rietzschel, T. Wagner, C. Funke, H.J. Möller, European Photovoltaic Solar Energy Conference and Excibition, Hamburg, Germany, 2009, 10.4229/24thEUPVSEC2009-2CV.1.49
[15] R. Guerrero-Lemus, R., Vega, R., Kim, T., Kimm, A. and Shephard, L.E., Renewable Sustainable Energy Rev., 2016 60, 1533–1549. Doi:10.1016/j.rser.2016.03.041.
[16] A.C. Pan, C. del Cañizo, A. Luque Proceedings of the Spanish conference on electron devices, Madrid, Spain, 2007, 234–237. DOI: 10.1109/sced.2007.384035.
[17] N. Dwivedi, S. Kumar, A. Bisht, K. Patel, S. Sudhakar, Solar Energy 88 (2013) 31–41, https://doi.org/10.1016/j.solener.2012.11.008.
[18] Data sheet, DOWANOL™ TPM Tripropylene Glycol Methyl Ether.
[19] J. Walters, K. Sunder, O. Anspach, R.P. Brooker, H. Seigneur, IEEE 43rd Photovoltaic Specialists Conference (PVSC), Portland, USA, 2016, pp. 0724-0728. doi: 10.1109/PVSC.2016.7749697.
[20] P.O. Maruschak, S.V. Panin, I.M. Zakiev, M.A. Poltaranin, A.L. Sotnikov, Eng. Failure Anal. 59 (2016) 69–78, https://doi.org/10.1016/j.engfailanal.2015.11.019.
[21] H.M. Princen, J. Colloid Interface Sci. 30 (1) (1969) 69–75, https://doi.org/10.1016/0021-9797(69)90379-8.
[22] H.M. Princen, J. Colloid Interface Sci. 30 (3) (1969) 359–371, https://doi.org/10.1016/0021-9797(69)90403-2.
[23] H.M. Princen, J. Colloid Interface Sci. 34 (2) (1970) 171–184, https://doi.org/10.1016/0021-9797(70)90167-0.
[24] H. Cooray, H.E. Huppert, J.A. Neufeld, Proc. R. Soc. A, 2016, 472, No. 2192. doi:10.1098/rspa.2016.0233
[25] Z.-H. Cheng, C.-K. Xu, R.-Q. Pei Proceedings of the Sixth International Conference on Machine Learning and Cybernetics, Hong Kong (2007) Doi: 10.1109/ICMLC.2007.4370241.
[26] L. Zhu, I. Kao, J. Sound Vibrat. 283 (2005) 589–620, https://doi.org/10.1016/j.jsv.2004.04.018.
[27] H. Huang, S. Wang, X. Xu, Mater. Sci. Semicond. Process 71 (2017) 93–101, https://doi.org/10.1016/j.mssp.2017.07.010.